



Rapid microwave synthesis of I-doped $\text{Bi}_4\text{O}_5\text{Br}_2$ with significantly enhanced visible-light photocatalysis for degradation of multiple parabens



Xin Xiao ^{a,*}, Mingli Lu ^a, Junmin Nan ^a, Xiaoxi Zuo ^a, Weide Zhang ^b, Shaomin Liu ^c, Shaobin Wang ^{c,*}

^a School of Chemistry and Environment, South China Normal University, Guangzhou, 510006, PR China

^b School of Chemistry and Chemical Engineering, South China University of Technology, Guangzhou, 510640, PR China

^c Department of Chemical Engineering, Curtin University, GPO Box U1987, Perth, WA 6845, Australia

ARTICLE INFO

Article history:

Received 7 May 2017

Received in revised form 19 June 2017

Accepted 23 June 2017

Available online 23 June 2017

Keywords:

Parabens

Photocatalysis

Visible light

I-doped $\text{Bi}_4\text{O}_5\text{Br}_2$

Mechanism

ABSTRACT

Parabens, a class of preservatives widely used in cosmetic and pharmaceutical products, are currently considered as potential emerging contaminants in the environment. Photocatalytic degradations of different parabens (methyl-, ethyl-, propyl-, and butylparaben) and their mixture were performed for the first time under visible-light irradiation using I-doped $\text{Bi}_4\text{O}_5\text{Br}_2$ photocatalysts, synthesized by a facile, fast, and energy-saving microwave route. Compared with pure $\text{Bi}_4\text{O}_5\text{Br}_2$, I-doped samples exhibited enhanced photocatalytic activities in the degradation of the parabens. $\text{I}_{0.7}\text{-}\text{Bi}_4\text{O}_5\text{Br}_2$ achieved the best performance, showing approximately 9.5, 10.4, 15.7, 24.2, and 27 times higher activities than those of $\text{Bi}_4\text{O}_5\text{Br}_2$ in the degradation of methylparaben, ethylparaben, propylparaben, butylparaben, and a mixture of parabens, respectively. The structures of the as-synthesized photocatalysts were carefully characterized, and the primary reactive oxygen species (ROS) in the photocatalytic process were identified. Photogenerated holes and superoxide radicals were found to be the key reactive species. Through doping with iodine, the valence-band potentials of the $\text{Bi}_4\text{O}_5\text{Br}_2$ photocatalysts were reduced, leading to decreases in their band-gap energies, while the separation efficiencies of the photogenerated carriers were significantly enhanced. Thus, I-doped $\text{Bi}_4\text{O}_5\text{Br}_2$ could absorb more visible-light and yield more superoxide radicals, resulting in excellent visible-light photodegradations of the parabens. In addition, the as-prepared $\text{I}_{0.7}\text{-}\text{Bi}_4\text{O}_5\text{Br}_2$ catalyst maintained a strong stability of photocatalytic performance, indicating its potential for practical applications.

© 2017 Elsevier B.V. All rights reserved.

1. Introduction

Paraoxybenzoic acid esters, which are often referred to as parabens, are a series of alkyl esters of p-hydroxybenzoic acid. Parabens have been used as preservatives since the 1920s [1]. Ever since then, they have been widely used as preservatives and antimicrobial agents in cosmetics, pharmaceuticals, foodstuffs, and other industrial products [2]. Commonly used parabens include methylparaben (MeP), ethylparaben (EtP), propylparaben (PrP), butylparaben (BuP), and their mixtures. The unique properties of parabens, such as broad-spectrum antibacterial activity, chemical stability, safe use, and low cost, make it relatively difficult to be replaced by other chemicals [3]. Due to the wide commercial

use of parabens, their residues are frequently detected in water resources [4], air, dust [5], soil, sediments [6], and even human serum, milk, placental tissue, and breast tumor tissue [7–9]. Previously, parabens have been classified as “generally regarded as safe” (GRAS) compounds and approved for use in food by the US Drug Administration (FDA) and the European Union (EU) [10]. Unfortunately, recent studies have revealed their estrogenic activity and carcinogenic potential [11–13]. As a result, parabens are now recognized as emerging environmental contaminants by the US Environmental Protection Agency (EPA) [14]. Therefore, it is necessary to develop effective methods to eliminate these preservative residues in the environment.

Thus far, common methods for the removal of parabens include traditional water treatment, biodegradation, and advanced oxidation processes (AOPs) [3]. The efficiency of parabens elimination in wastewater treatment plants has been claimed to be up to 96% [15]. However, parabens have been frequently detected in the effluents

* Corresponding authors.

E-mail addresses: xiaox@scnu.edu.cn (X. Xiao), Shaobin.wang@curtin.edu.au, shaobin.wang@exchange.curtin.edu.au (S. Wang).

of wastewater as well as in other aquatic media at nanograms to micrograms per liter. This indicates the inefficiency of traditional water treatment for the removal of parabens, thus more efficient techniques for their complete removal are critical. The simplicity, high degradation efficiency, and absence of post-treatment make AOPs more appropriate and advantageous options for the removal of a wide variety of organic contaminants in the environment [16,17].

Recently, several studies using photocatalytic processes for the removal of single paraben in aqueous solutions were reported. For instance, Lin and coworkers investigated the removal of MeP or benzylparaben using TiO_2 as a catalyst under ultraviolet-light irradiation [14,18]. Photocatalysis based on TiO_2 and UV light was also employed to degrade PrP and BuP [19,20]. In addition, Athanasia et al. studied the kinetics of EtP elimination under simulated solar irradiation in the presence of N-doped TiO_2 [21]. However, few studies on the degradation of various parabens and their mixtures using photocatalytic processes under visible-light, which accounts for more than 44% of solar radiation, have been explored.

For photocatalyst systems, the intrinsic polarizability induced by the Bi 6s² lone pair of electrons favors the separation and transformation of photogenerated electron-hole pairs [22] and many bismuth-based semiconductors, such as Bi_2O_3 , BiVO_4 , Bi_2WO_6 , Bi_2MoO_6 , $\text{Bi}_{12}\text{TiO}_{20}$, $\text{Bi}_2\text{Fe}_4\text{O}_9$, Bi_3NbO_7 , and NaBiO_3 , have been found to be visible-light-driven photocatalysts with high activities [23,24]. Recently, bismuth oxyhalides (BiOX , X=Cl, Br, and I) and their composites have proved excellent visible-light photocatalytic performances owing to their efficient photogenerated charges separation, excellent stability, and broad tunable band gaps [25–29]. In previous works, we first reported that MeP and PrP could be photocatalytically degraded by $\beta\text{-Bi}_2\text{O}_3$ and $\text{Bi}_4\text{O}_5\text{I}_2/\text{Bi}_5\text{O}_7\text{I}$, respectively, under visible-light irradiation [30,31]. A further study revealed that the removal of parabens in aqueous solution through visible-light-induced photocatalytic processes is not easy because of the relatively high oxidation potentials of parabens originating from their carboxyl groups. $\text{Bi}_4\text{O}_5\text{Br}_2$ was proven to have sufficient thermodynamics for photocatalytic degradation of parabens under visible light due to its sufficient positive valence potential, effective visible-light absorption, and structural stability [32]. However, additional efforts are required to further improve its capability in degradation efficiency and capacity for the elimination of different types and mixtures of parabens.

In this work, novel I-doped $\text{Bi}_4\text{O}_5\text{Br}_2$ photocatalysts with different iodine contents were successfully synthesized via a facile microwave synthesis route. The effects of iodine doping on the composition, structure, morphology, photoabsorption, specific surface area, and band structure compared with pure $\text{Bi}_4\text{O}_5\text{Br}_2$ were analyzed. The photocatalytic degradations of four parabens (MeP, EtP, PrP, and BuP) and a mixture of MeP and PrP over the as-synthesized I-doped $\text{Bi}_4\text{O}_5\text{Br}_2$ were then investigated under visible-light irradiation. The band structures and photogenerated carrier separation capabilities of the as-synthesized photocatalysts were comprehensively investigated by theoretical calculations and physicochemical characterizations, and the roles of photogenerated primary oxidative species in the process were identified. Then, a possible photocatalytic mechanism in this process was proposed.

2. Experimental

2.1. Materials and methods

Methylparaben (MeP), ethylparaben (EtP), propylparaben (PrP), and butylparaben (BuP) were obtained from J&K Chemical Ltd. Bismuth nitrate pentahydrate ($\text{Bi}(\text{NO}_3)_3 \cdot 5\text{H}_2\text{O}$), potassium bromide (KBr), and potassium iodide (KI) were purchased from Tianjin Ker-

mel Chemical Reagent Co. Ltd. Ethylene glycol (EG) was obtained from Chinasun Specialty Products Co. Ltd. All the chemicals were of analytical grade and used as received without further purification.

$\text{Bi}_4\text{O}_5\text{Br}_2$ and I-doped $\text{Bi}_4\text{O}_5\text{Br}_2$ were synthesized using a facile and rapid microwave method. In a typical procedure, 1 mmol $\text{Bi}(\text{NO}_3)_3 \cdot 5\text{H}_2\text{O}$ was dissolved completely in 50 mL ethylene glycol at room temperature using a 150 mL round flask as the container. Then, 0.5 mmol KBr was added in the solution under stirring condition. After 15 min, a certain amount of KI (molar ratio of I/Br varied from 0.2 to 1) was added to the solution. After vigorously stirring for another 15 min, the reaction was performed in a microwave chemical reactor (MCR-3, at a fixed frequency of 2.45 GHz and the maximum output of 800 W, Beijing Rui Cheng Wei Industry Equipment Co. Ltd., China) at 400 W for 4 min equipped with in situ magnetic stirring and condensing apparatus. After the reaction, the mixture was continuously stirring for another 30 min until its temperature dropped down. Then, the precipitate was collected by centrifugation, washed with distilled water and ethanol for several times and finally dried in an oven at 60 °C overnight. The samples with a different KI addition were labeled as $\text{I}_x\text{-Bi}_4\text{O}_5\text{Br}_2$ (x is the molar feed ratio of I/Br, $x=0.2, 0.4, 0.6, 0.7, 0.8$, and 1). Pure $\text{Bi}_4\text{O}_5\text{Br}_2$ was prepared by the same procedure except that KI was not added into the reaction system (i.e. $x=0$).

For further comparison, three other $\text{Bi}_4\text{O}_5\text{Br}_2$ samples were also prepared by a molecular precursors' hydrolysis process [33], a one-step hydrolysis route [34], and an ionic liquids-assisted solvothermal method [35] according to literatures, and were denoted as S1–S3, respectively. In addition, $\text{Bi}_4\text{O}_5\text{Br}_x\text{I}_{2-x}$ solid solutions with different molar Br/I ratio were synthesized according to previously reported method [36].

2.2. Catalyst characterizations

The composition and structure of the as-synthesized samples were determined by powder X-ray diffraction (XRD) using a Bruker D8 Advance X-ray diffractometer (Bruker AXS, Germany) with a Cu-K α radiation source. The morphologies of samples were observed by field-emission scanning electron microscopy (FE-SEM, Zeiss Ultra 55, Germany). Chemical elemental mapping was performed by combining the scanning module of the microscope with an energy dispersive X-ray spectroscopy (EDX) detector. The surface compositions were analyzed using X-ray photoelectron spectroscopy (XPS, Kratos Axis Ultra DLD) equipped with an Al-K α source. UV-vis diffuse reflectance spectra (DRS) were recorded on a UV-vis spectrophotometer (UV-3010, Hitachi, Japan) using BaSO_4 as a reference, and the spectra were converted from reflectance to absorbance by the Kubelka-Munk method. The specific surface areas of the samples were measured by nitrogen adsorption-desorption isotherms according to the Brunauer-Emmett-Teller method (BET, ASAP 2020, Micromeritics, USA) at –196 °C. A desorption isotherm was applied to calculate the pore-size distribution using the Barrett-Joyner-Halenda (BJH) method. Electron paramagnetic resonance (EPR, JES FA-200, JEOL, Japan) in combination with spin-trapping techniques was utilized to detect free radicals using 5,5-dimethyl-1-pyrroline-N-oxide (DMPO) as a spin trap under visible-light irradiation ($\lambda > 420$ nm) using a xenon lamp coupled with a filter as a light source. Photocurrent measurements were performed with a CHI 660C electrochemical station (Chenhua Instruments Co. Shanghai, China) in a standard three-electrode configuration with the as-prepared samples as the working electrodes, a platinum plate as the counter electrode, and a commercial Ag/AgCl electrode as the reference electrode. The electrolyte used was a 0.5 M Na_2SO_4 aqueous solution. A 300-W xenon lamp (PLS-SXE300-300UV) assembled with a UV-light cut-off filter was used as the visible-light ($\lambda > 420$ nm) irradiation source.

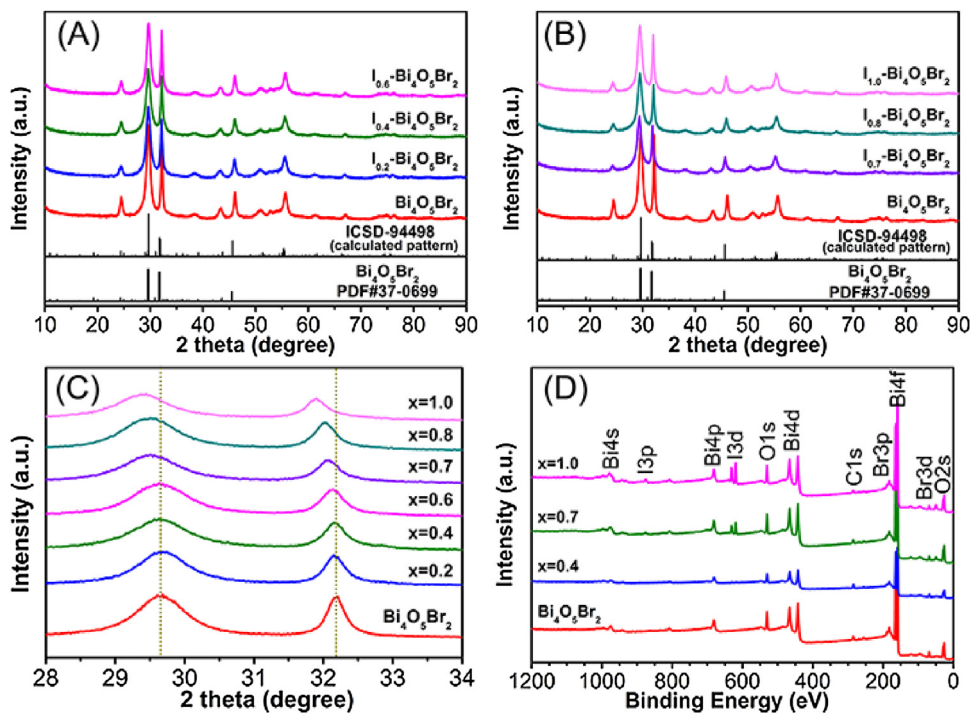


Fig. 1. (A–C) XRD patterns of as-synthesized Bi₄O₅Br₂ and I_x-Bi₄O₅Br₂ (x = 0.2, 0.4, 0.6, 0.7, 0.8, and 1.0); (D) XPS spectra of as-synthesized Bi₄O₅Br₂ and I_x-Bi₄O₅Br₂ (x = 0.4, 0.7, and 1.0).

2.3. Photocatalytic activity measurements

The photocatalytic degradation experiments of single or mixture of parabens over the as-prepared photocatalysts were performed in a photochemical reactor (XPA-VII, Nanjing Xujiang Machine-electronic Plant, China) equipped with a 1000 W xenon lamp with a UV-light cut-off filter as the visible-light source ($\lambda > 420$ nm). In each experiment, 50 mg of the as-synthesized photocatalyst was added into 50 mL of the reaction solution with an initial concentration of 10 mg L⁻¹. The reaction solution was consisted of MeP, EtP, PrP, BuP, or a mixture of MeP and PrP with a concentration ratio of 1:3 as in practical solution. Prior to irradiation, the reaction suspension was stirred for 1 h in dark for an adsorption-desorption equilibrium. During the photocatalytic process, approximately 2.5 mL of the suspension was taken out at specified time, filtered using a 0.45- μ m nitrocellulose filter, and the paraben concentration was measured by recording the absorbance at 255 nm using UV-vis spectroscopy (UV-1800, Shimadzu, Japan). The concentrations of MeP and PrP in the mixed solutions were quantified using high-performance liquid chromatography (HPLC, Shimadzu SCL-6A, Japan) with an ultraviolet detector, a Waters C-18 reverse-phase column (5 mm \times 150 mm \times 3.9 mm), a mobile phase of methanol and water at a ratio of 60:40 (v/v) in an injection rate of 1 mL min⁻¹, and an oven temperature of 35 °C. Two peaks were well defined at retention time of 5.8 and 12.5 min corresponding to MeP and PrP, respectively. Total organic carbon (TOC) was estimated by an automatic total organic carbon analyzer (TOC-V, Shimadzu, Japan).

Photocatalytic reduction of CO₂ experiments were carried out in a quartz reaction cell irradiated by a 300 W high-pressure Xenon lamp (PLS-SXE300C, Beijing Perfectlight Technology Co. Ltd. China.) equipped with a 420 nm filter. Every 1 mL of gas was taken from the reaction cell at interval times for qualitative analysis using an Agilent 7890B gas chromatograph equipped with a flame ionization detector (FID) and a thermal conductivity detector (TCD).

2.4. Theoretical calculations

The calculations of band structures and density of states (DOS) of pure Bi₄O₅Br₂ and I-doped Bi₄O₅Br₂ were investigated based on density functional theory (DFT) through the plane-wave-pseudopotential approach. The crystal data for Bi₄O₅Br₂ (ICSD #94498) were utilized as the original crystal model. Then, their electronic structures were calculated within the generalized gradient approximation (GGA-PBE), as implemented in the highly efficient Cambridge serial total energy package (CASTEP) code. The k-point meshes for Brillouin zone sampling were constructed using the Monkhorst-Pack scheme. A plane-wave cut-off energy of 380 eV was used. Then, the energy band and electronic structures were calculated based on the optimized geometries.

The energies of the highest occupied molecular orbital (HOMO) and the lowest unoccupied molecular orbital (LUMO) of the four parabens (MeP, EtP, PrP, and BuP) were calculated via density functional theory (DFT) using Gaussian 09 software. The B3LYP functional and the 6-311++G (d, p) basis set were used to acquire the optimized geometries and energies.

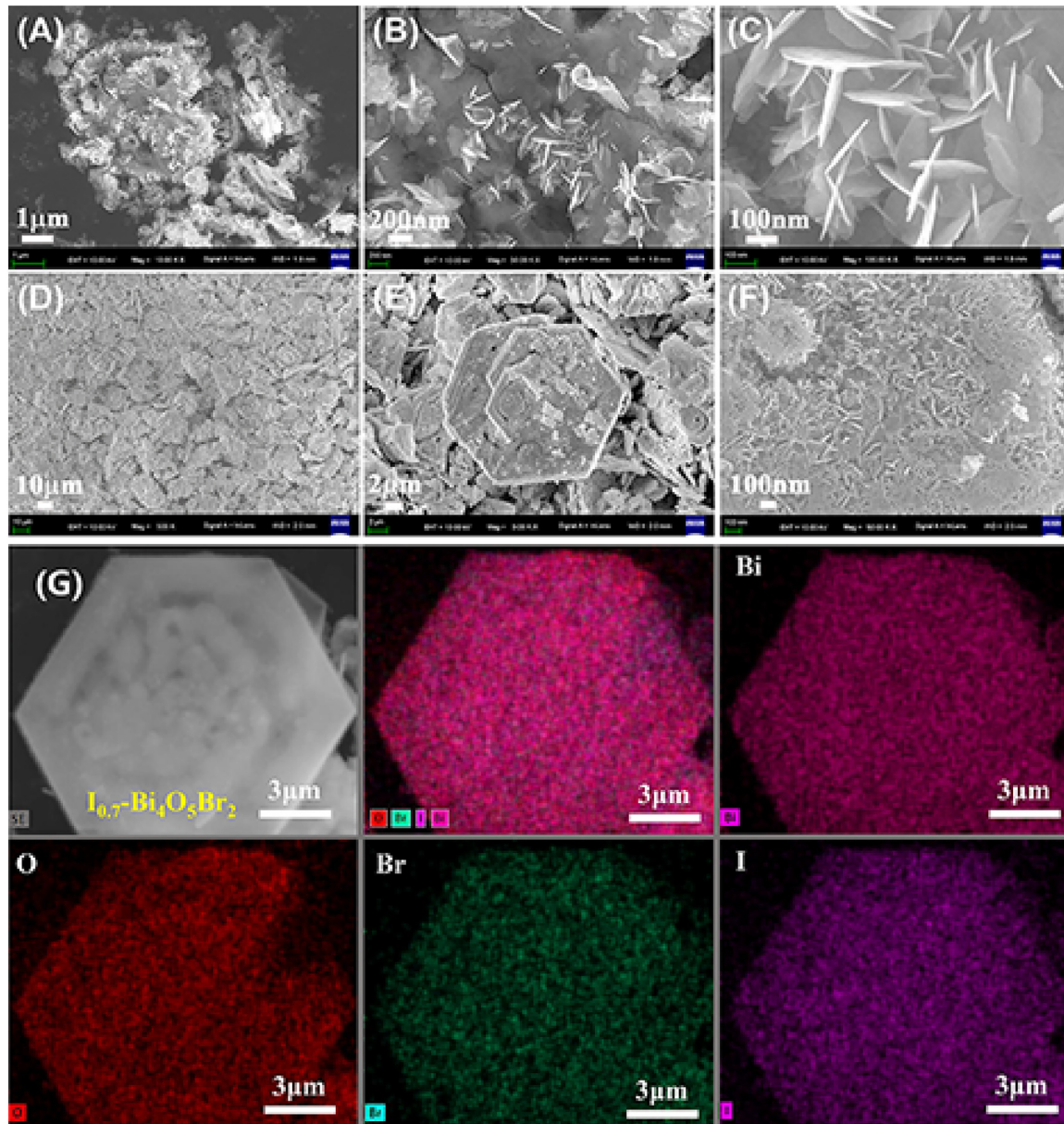
3. Results and discussion

3.1. Characterization of the photocatalysts

XRD was used to identify the phase composition of the as-prepared products. As shown in Fig. 1A and B, the diffraction peaks of the sample synthesized without KI was indexed as monoclinic Bi₄O₅Br₂ (JCPDS NO. 37-0699), which can be further confirmed by the diffraction pattern calculation from the crystal structure of Bi₄O₅Br₂ (ICSD #94498). Compared to the pure Bi₄O₅Br₂, the diffraction peaks of the I-doped Bi₄O₅Br₂ samples were slightly different, indicating that the structures did not significantly change after the iodine doping. The diffraction peaks are slightly shifted to lower 2 θ values with an increasing iodine amount (Fig. 1C). According to Bragg's law: $d_{hkl} = \lambda / (2 \sin \theta)$, where d_{hkl} is the distance

Table 1Physicochemical properties of four typical $I_x\text{-Bi}_4\text{O}_5\text{Br}_2$ samples.

I:Br (feeding ratio)	I:Br (XPS analysis)	Bi:(Br+I) (XPS analysis)	BET surface area (m^2g^{-1})	Band gap (eV) (DRS analysis)
0	0	1.99	23.9	2.62
0.4	0.12	1.98	36.5	2.58
0.7	0.42	2.05	34.2	2.51
1.0	0.68	1.85	37.3	2.41

**Fig. 2.** SEM images of as-synthesized $\text{Bi}_4\text{O}_5\text{Br}_2$ (A–C) and $I_{0.7}\text{-}\text{Bi}_4\text{O}_5\text{Br}_2$ (D–F); SEM-EDX mapping of the as-synthesized $I_{0.7}\text{-}\text{Bi}_4\text{O}_5\text{Br}_2$ (G).

between the crystal planes of (hkl) , λ is the X-ray wavelength, and θ is the diffraction angle of the crystal plane (hkl) [37], the observed shift of the peaks towards lower 2θ could be ascribed to the gradual substitution of Br by I since the radius of I^- (0.216 nm) is larger than that of Br^- (0.195 nm), which would lead to an enlarged lattice.

The as-synthesized $\text{Bi}_4\text{O}_5\text{Br}_2$, $I_{0.4}\text{-}\text{Bi}_4\text{O}_5\text{Br}_2$, $I_{0.7}\text{-}\text{Bi}_4\text{O}_5\text{Br}_2$, and $I_{1.0}\text{-}\text{Bi}_4\text{O}_5\text{Br}_2$ were also investigated by XPS, as shown in Fig. 1D. $\text{Bi}_4\text{O}_5\text{Br}_2$ is composed of Bi, O, Br, and a trace amount of C (adventitious carbon), and the peak of I becomes increasingly noticeable with an increasing content of the iodine in $I_x\text{-}\text{Bi}_4\text{O}_5\text{Br}_2$, revealing

that I was successfully added into the products. A quantitative analysis of XPS was performed to determine the I/Br and Bi/(Br+I) ratios in these samples, as summarized in Table 1. The ratio of I/Br grows significantly with more I added, while the Bi/(Br+I) ratio remains similarly at 2 to keep a basic composition of $\text{Bi}_4\text{O}_5\text{X}_2$ ($\text{X} = \text{Br} + \text{I}$). However, the molar I/Br ratio in the samples from the XPS analysis is obviously less than the feeding ratio, suggesting Br dominates the composition of the final products and I can partially substitute Br. This is probably associated with the fact that $\text{Bi}_4\text{O}_5\text{Br}_2$ is more easily formed in the rapid microwave reaction [38,39].

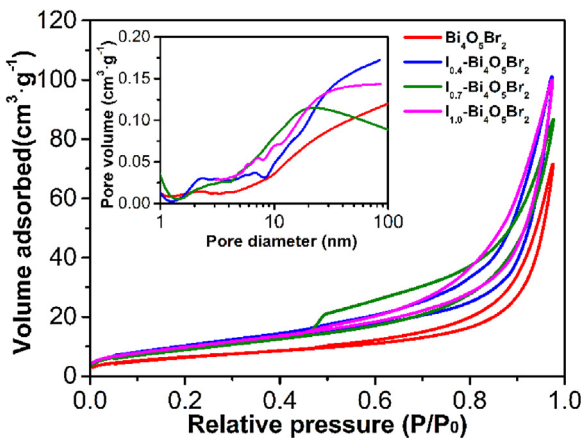


Fig. 3. Nitrogen adsorption-desorption isotherms and pore-size distribution curves (inset) of $\text{Bi}_4\text{O}_5\text{Br}_2$ and $\text{I}_x\text{-}\text{Bi}_4\text{O}_5\text{Br}_2$ ($x = 0.4, 0.7$, and 1.0).

The morphologies and surface structures of the as-synthesized $\text{Bi}_4\text{O}_5\text{Br}_2$ and $\text{I}_{0.7}\text{-}\text{Bi}_4\text{O}_5\text{Br}_2$ samples were analyzed by SEM. The pure $\text{Bi}_4\text{O}_5\text{Br}_2$ sample consists of many nanoflakes with a thickness of about 5 nm and the lengths and widths of the nanoflakes are approximately 400 nm (Fig. 2A–C). After iodide doping, the as-prepared $\text{I}_{0.7}\text{-}\text{Bi}_4\text{O}_5\text{Br}_2$ sample (Fig. 2D–F) presents in microplate structures resembling polygonal shapes with widths of 20–40 μm and thickness of 1 μm . A close observation revealed numerous nanoflakes grown on the surfaces of the microplates, forming a special micro/nano-hierarchical architecture. Scanning electron microscopy-energy dispersive X-ray (SEM-EDX) analysis reveals that Bi, O, Br, and I are uniformly distributed on the $\text{I}_{0.7}\text{-}\text{Bi}_4\text{O}_5\text{Br}_2$ sample surface (Fig. 2G), further confirming that the as-synthesized product is composed of homogeneous I-doped $\text{Bi}_4\text{O}_5\text{Br}_2$ instead of a mixture of different compounds.

It is widely accepted that a photocatalyst with a large specific surface area could offer more active reaction sites and provide extra interfaces for interactions between the catalysts and pollutants, thus leading to a superior photocatalytic performance. The nitrogen adsorption-desorption isotherms of $\text{Bi}_4\text{O}_5\text{Br}_2$, $\text{I}_{0.4}\text{-}\text{Bi}_4\text{O}_5\text{Br}_2$, $\text{I}_{0.7}\text{-}\text{Bi}_4\text{O}_5\text{Br}_2$, and $\text{I}_{1.0}\text{-}\text{Bi}_4\text{O}_5\text{Br}_2$ are shown in Fig. 3. All the isotherms are of type IV with a H3 hysteresis loop, indicating their mesoporous features. The surface areas were estimated using the BET method to be 23.9, 36.5, 34.2, and $37.3 \text{ m}^2 \text{ g}^{-1}$ for $\text{Bi}_4\text{O}_5\text{Br}_2$, $\text{I}_{0.4}\text{-}\text{Bi}_4\text{O}_5\text{Br}_2$, $\text{I}_{0.7}\text{-}\text{Bi}_4\text{O}_5\text{Br}_2$, and $\text{I}_{1.0}\text{-}\text{Bi}_4\text{O}_5\text{Br}_2$, respectively. The iodine-doped samples have larger specific surface areas than that of pure $\text{Bi}_4\text{O}_5\text{Br}_2$, which is mainly attributed to the presence of micro/nano-hierarchical architectures assembled by the nanoflakes on the I-doped $\text{Bi}_4\text{O}_5\text{Br}_2$ samples, but the amount of iodine had little effect on the specific surface area. The pore-size distributions of the as-prepared $\text{Bi}_4\text{O}_5\text{Br}_2$ and I-doped $\text{Bi}_4\text{O}_5\text{Br}_2$ were determined using the BJH method (inset of Fig. 3), revealing that all the samples possessed mesoporous-macroporous structures with broad pore distributions, which most likely arises from their inter-nanoflake spaces.

The band structure of a semiconductor is considered as one of the key factors determining its photocatalytic performance. Fig. 4 shows the UV-vis diffuse reflectance spectra (DRS) of the as-prepared $\text{Bi}_4\text{O}_5\text{Br}_2$ and three typical I-doped $\text{Bi}_4\text{O}_5\text{Br}_2$ samples. The absorbance edge of pure $\text{Bi}_4\text{O}_5\text{Br}_2$ is approximately at 486 nm, while the I-doped $\text{Bi}_4\text{O}_5\text{Br}_2$ sample shows a redshift towards the visible-light region with an increasing iodine content. The maximum absorbance wavelengths of $\text{I}_{0.4}\text{-}\text{Bi}_4\text{O}_5\text{Br}_2$, $\text{I}_{0.7}\text{-}\text{Bi}_4\text{O}_5\text{Br}_2$, and $\text{I}_{1.0}\text{-}\text{Bi}_4\text{O}_5\text{Br}_2$ are extended to approximately 494, 510, and 530 nm, respectively. Correspondingly, the samples display various colors ranging from beige white to brilliant yellow, and the color gradu-

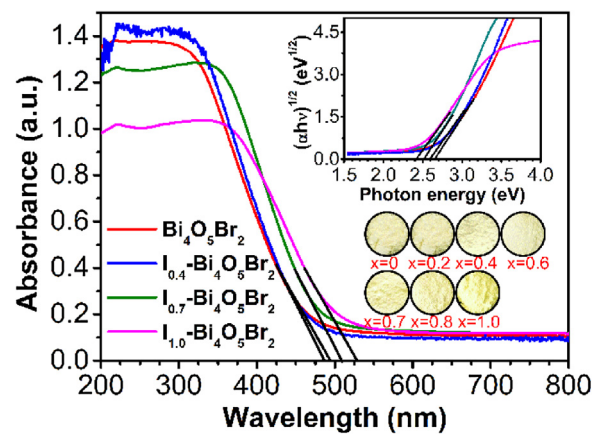


Fig. 4. UV-vis diffuse reflectance spectra of $\text{Bi}_4\text{O}_5\text{Br}_2$ and I-doped $\text{Bi}_4\text{O}_5\text{Br}_2$; the circular insets show the corresponding digital photos of the as-synthesized samples; inset: plots of $(\alpha h\nu)^{1/2}$ vs. photon energy ($h\nu$).

ally increases in intensity with an increasing iodine content (inset of Fig. 4). The band-gap energies of these samples can be determined by the following equation (Eq. (1)) [40]:

$$\alpha(h\nu) = A(h\nu - E_g)^n/2 \quad (1)$$

where α , ν , E_g and A are the absorption coefficient, light frequency, band-gap energy, and a constant, respectively, and n is related to the characteristics of the transition in the semiconductor. For $\text{Bi}_4\text{O}_5\text{Br}_2$ semiconductors, n is 4 due to its indirect transition [41]. The band-gap energies (E_g) of $\text{Bi}_4\text{O}_5\text{Br}_2$, $\text{I}_{0.4}\text{-}\text{Bi}_4\text{O}_5\text{Br}_2$, $\text{I}_{0.7}\text{-}\text{Bi}_4\text{O}_5\text{Br}_2$, and $\text{I}_{1.0}\text{-}\text{Bi}_4\text{O}_5\text{Br}_2$ were estimated to be 2.62, 2.58, 2.51, and 2.41 eV, respectively, indicating that a reduction of the band-gap energy and an expansion of the light-absorption capacity occur with more iodine doping. The E_g value of $\text{Bi}_4\text{O}_5\text{Br}_2$ in this study is similar to the previously reported value [42], while all I-doped $\text{Bi}_4\text{O}_5\text{Br}_2$ samples have much larger E_g values than that of pure $\text{Bi}_4\text{O}_5\text{Br}_2$ (value = 2.17 eV) [43].

The effects of iodine doping on the electronic and band structures of $\text{Bi}_4\text{O}_5\text{Br}_2$ and I-doped $\text{Bi}_4\text{O}_5\text{Br}_2$ (with 25% I and 75% Br, $\text{I}/\text{Br} = 0.33$) were theoretically calculated according to their crystal structure models (Fig. 5A and B) using density functional theory (DFT) and the GGA-PBE function. As shown in Fig. 5C, the band-gap energies of $\text{Bi}_4\text{O}_5\text{Br}_2$ and I-doped $\text{Bi}_4\text{O}_5\text{Br}_2$ were obtained to be 2.447 and 2.325 eV, respectively, which are slightly lower than the results from DRS measurements. In addition, the conduction band (CB) of $\text{Bi}_4\text{O}_5\text{Br}_2$ is mainly composed of Bi 6p, Br 4s, and O 2p orbitals, and the valence band (VB) is dominated by O 2p, Br 4p, and Bi 6s states. When a portion of bromine in $\text{Bi}_4\text{O}_5\text{Br}_2$ is replaced by iodine, I 5p states are also involved in the VB, which mainly causes a reduced band gap from pure $\text{Bi}_4\text{O}_5\text{Br}_2$ to I-doped $\text{Bi}_4\text{O}_5\text{Br}_2$. The theoretical speculation can be further validated by valence-band XPS (VB XPS) measurements. As shown in Fig. 5D, with an increase in the iodine content, the VB energy of these samples continuously decreases. Moreover, the composition of the s orbitals in the hybridized CB increases obviously after iodine doping, which may lead to a high mobility of photogenerated carriers due to the dispersive characteristic of the s orbitals and thus favor the separation of photoinduced electron-hole pairs.

3.2. Photocatalytic degradation of single and mixed parabens

Propylparaben (PrP), one of the most commonly used parabens [44], was chosen as the initial model to estimate the visible-light photocatalytic activities of the as-synthesized I-doped $\text{Bi}_4\text{O}_5\text{Br}_2$ samples (Fig. 6). All the catalyst samples possessed a certain ability to degrade PrP. After irradiation for 60 min, the degradation effi-

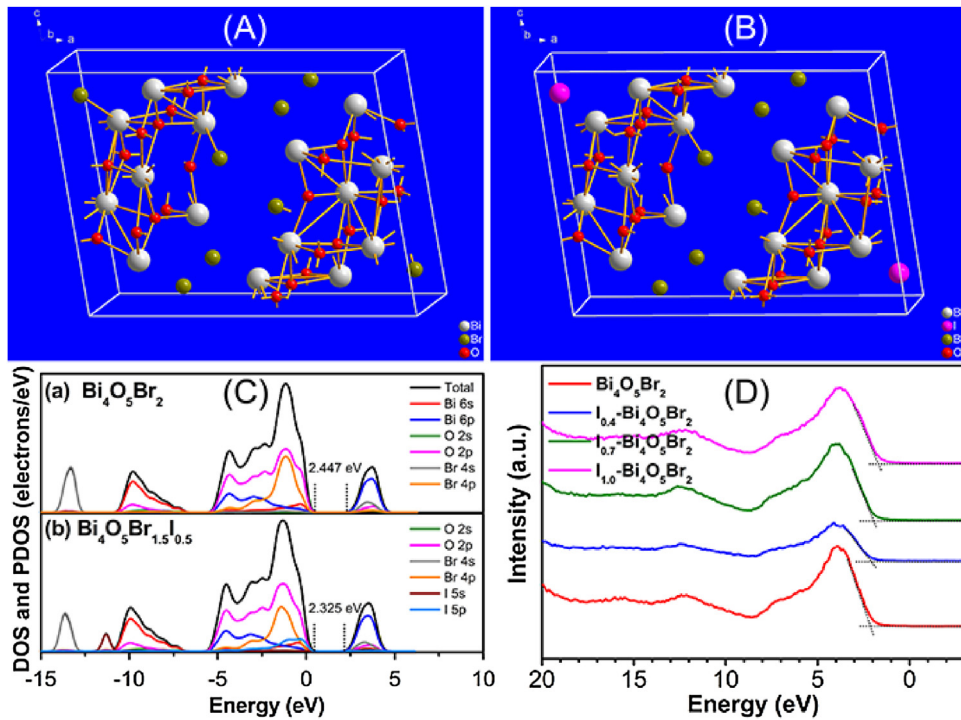


Fig. 5. The crystal structures of (A) $\text{Bi}_4\text{O}_5\text{Br}_2$ (ICSD #412591) and (B) I-substituted $\text{Bi}_4\text{O}_5\text{Br}_2$ (with 25% I and 75% Br); (C) band structures and partial density of states (PDOS) of $\text{Bi}_4\text{O}_5\text{Br}_2$ and $\text{Bi}_4\text{O}_5\text{Br}_{1.5}\text{I}_{0.5}$; (D) VB XPS spectra of as-synthesized $\text{Bi}_4\text{O}_5\text{Br}_2$ and $\text{I}_x\text{-}\text{Bi}_4\text{O}_5\text{Br}_2$ ($x = 0.4, 0.7$, and 1.0).

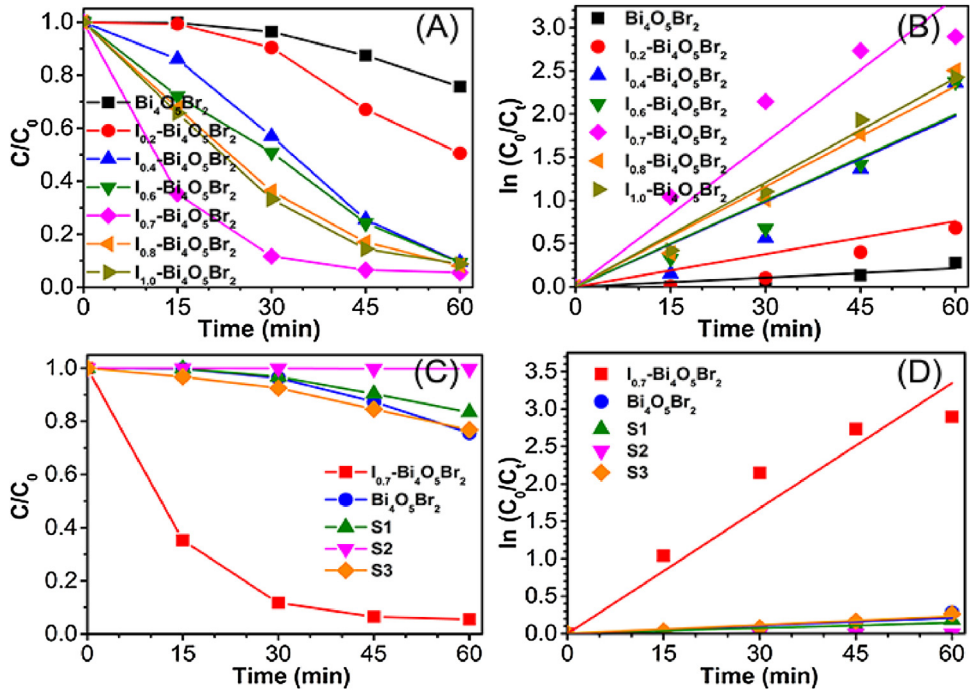


Fig. 6. (A) Photocatalytic degradation of propylparaben over $\text{Bi}_4\text{O}_5\text{Br}_2$ and I-doped $\text{Bi}_4\text{O}_5\text{Br}_2$ under visible-light irradiation; (B) the linear plots of $\ln(\text{C}_0/\text{C}_t)$ versus degradation time; (C) the comparison of the photocatalytic degradation of propylparaben over $\text{I}_{0.7}\text{-}\text{Bi}_4\text{O}_5\text{Br}_2$ and four $\text{Bi}_4\text{O}_5\text{Br}_2$ samples synthesized via different methods.

iciencies were 24.4%, 49.4%, 90.6%, 90.7%, 94.5%, 91.8%, and 91.2%, for $\text{Bi}_4\text{O}_5\text{Br}_2$ and $\text{I}_x\text{-}\text{Bi}_4\text{O}_5\text{Br}_2$ ($x = 0.2, 0.4, 0.6, 0.7, 0.8$, and 1.0), respectively. The iodine doping can significantly improve the photocatalytic efficiency, and a higher content of iodine in the sample led to a better photocatalytic activity up to I/Br at 0.7. When the atom feeding ratio of I/Br exceeded 0.7, the photocatalytic performance of I-doped $\text{Bi}_4\text{O}_5\text{Br}_2$ was not further improved and even

decreased. Their reaction kinetics were analyzed by fitting the data to a pseudo-first-order kinetic equation (Eq. (2)) [45]:

$$-\ln\left(\frac{\text{C}_t}{\text{C}_0}\right) = k_{\text{app}} t \quad (2)$$

where k_{app} is the apparent reaction rate constant (min^{-1}), t is the irradiation time (min), C_0 is the initial concentration of PrP, and C_t is the concentration of PrP at time t . It was found from Fig. 6B

Table 2

The k_{app} values of the visible-light photocatalytic degradation of single or a mixture of parabens over the as-synthesized $\text{Bi}_4\text{O}_5\text{Br}_2$ and I-doped $\text{Bi}_4\text{O}_5\text{Br}_2$ photocatalysts.

Catalyst	MeP	EtP	PrP	BuP	MeP (in mixture)	PrP (in mixture)
$\text{Bi}_4\text{O}_5\text{Br}_2$	0.00471	0.00593	0.00356	0.00274	0.00176	0.00118
$\text{I}_{0.4}\text{-}\text{Bi}_4\text{O}_5\text{Br}_2$	0.0136	0.0226	0.0329	0.0190	0.00185	0.00163
$\text{I}_{0.7}\text{-}\text{Bi}_4\text{O}_5\text{Br}_2$	0.0449	0.0618	0.0558	0.0662	0.0479	0.0560
$\text{I}_{1.0}\text{-}\text{Bi}_4\text{O}_5\text{Br}_2$	0.0368	0.0526	0.0403	0.0380	0.0340	0.0450

that the plots are linear with good correlation coefficients, indicating that the photodegradation data are matched well with the pseudo first-order rate equation. Accordingly, the k_{app} values of $\text{Bi}_4\text{O}_5\text{Br}_2$ and $\text{I}_x\text{-}\text{Bi}_4\text{O}_5\text{Br}_2$ ($x = 0.2, 0.4, 0.6, 0.7, 0.8$, and 1.0) were calculated to be $0.00356, 0.0127, 0.0330, 0.0333, 0.0558, 0.0403$, and 0.0387 min^{-1} , respectively. $\text{I}_{0.7}\text{-}\text{Bi}_4\text{O}_5\text{Br}_2$ exhibited a degradation rate of approximately 15.7 times higher than that of pure $\text{Bi}_4\text{O}_5\text{Br}_2$. Moreover, three other $\text{Bi}_4\text{O}_5\text{Br}_2$ samples (labelled as S1–S3) were synthesized according to molecular-precursor hydrolysis [33], one-step hydrolysis [34], and ionic-liquid-assisted solvothermal method [35], respectively. Their photocatalytic activities for the degradation of PrP were estimated under the same conditions, as shown in Fig. 6C and D. The activities of these $\text{Bi}_4\text{O}_5\text{Br}_2$ samples did not show any noticeable enhancements compared to the activities of the microwave-synthesized samples, which further confirms that the performances of the I-doped $\text{Bi}_4\text{O}_5\text{Br}_2$ samples are excellent compared to the pure $\text{Bi}_4\text{O}_5\text{Br}_2$ samples.

Based on a hybrid halogen strategy and molecular precursor method, Yang et al. successfully synthesized $\text{Bi}_4\text{O}_5\text{Br}_x\text{I}_{2-x}$ solid solutions [36] and showed their superb photocatalytic activities for CO_2 conversion and Cr(VI) reduction under visible-light. We thus employed the similar method to prepare five samples of $\text{Bi}_4\text{O}_5\text{Br}_x\text{I}_{2-x}$ solid solutions in different molar Br/I ratios and tested their photocatalytic activities for degradation of propylparaben under the identical conditions as I-doped $\text{Bi}_4\text{O}_5\text{Br}_2$ samples. All the $\text{Bi}_4\text{O}_5\text{Br}_x\text{I}_{2-x}$ samples exhibited very poor photocatalytic oxidation performances (Fig. S1, Supporting Information). Meanwhile, $\text{I}_{0.7}\text{-}\text{Bi}_4\text{O}_5\text{Br}_2$ sample presented a very low CO_2 reduction efficiency with trace CO generation (not shown here). The above investigations reveal different catalytic behaviors of I-doped $\text{Bi}_4\text{O}_5\text{Br}_2$ and $\text{Bi}_4\text{O}_5\text{Br}_x\text{I}_{2-x}$ solid solutions. $\text{Bi}_4\text{O}_5\text{Br}_x\text{I}_{2-x}$ solid solution exhibited photocatalytic reduction activity with thermodynamically favorable energy band structure and better light absorption capacity. However, $\text{Bi}_4\text{O}_5\text{Br}_2$ itself owns an appropriate energy band structure for effective degradation of parabens [32]. Adding iodine into $\text{Bi}_4\text{O}_5\text{Br}_2$ will build a new energy level in the band structure and produce structural defects to extend the photogenerated carrier lifetime and separation efficiency as well as to improve its light absorption by reducing its bandgap energy, which results in a superior photocatalytic oxidation activity for the organic pollutants removal.

In addition to PrP, three other parabens, including MeP, EtP, and BuP, are also widely used in industries. The removal of these four parabens within a single oxidation process was reported [2,46,47], yet the investigation of a photocatalytic system to effectively eliminate these four parabens has not been investigated. Therefore, the degradations of MeP, EtP, and BuP were also evaluated over the as-prepared $\text{Bi}_4\text{O}_5\text{Br}_2$ and three typical $\text{I}_x\text{-}\text{Bi}_4\text{O}_5\text{Br}_2$ ($x = 0.4, 0.7$, and 1.0) samples under the identical conditions (Fig. 7A–C). The degradation activities over I-doped $\text{Bi}_4\text{O}_5\text{Br}_2$ for the other three parabens are obviously higher than those of pure $\text{Bi}_4\text{O}_5\text{Br}_2$. The corresponding linear plots of $\ln(C_0/C_t)$ versus degradation time are presented in Fig. 7D–F, and the k_{app} values were evaluated and summarized in Table 2. According to the results, significant enhancements were found for the $\text{I}_{0.7}\text{-}\text{Bi}_4\text{O}_5\text{Br}_2$ sample in all the cases, which showed approximately 9.5, 10.4, 24.2 times higher

Table 3

Theoretical calculations of the molecular orbital energies of four parabens.

Paraben	E_{HOMO} /eV	E_{LUMO} /eV	$\Delta E_{\text{L-H}}$ /eV	Oxidation potential (V)
MeP	-6.319	-0.927	5.392	1.819
EtP	-6.294	-0.893	5.401	1.794
PrP	-6.288	-0.885	5.403	1.788
BuP	-6.279	-0.876	5.403	1.779

activity than pure $\text{Bi}_4\text{O}_5\text{Br}_2$ in the degradation of MeP, EtP, and BuP, respectively.

From the results, $\text{Bi}_4\text{O}_5\text{Br}_2$ presents better degradation of MeP and EtP than PrP and BuP while I-doped $\text{Bi}_4\text{O}_5\text{Br}_2$ can significantly improve the degradation of PrP and BuP, suggesting their advantages for degradation of all parabens.

With an increase in the length of the alkyl group, the antibacterial activity of the parabens increases, while their aqueous solubility decreases. Practically, a mixture of parabens is generally used to enhance the antibacterial effect. The photocatalytic removal of a mixture of MeP and PrP (concentration ratio of 1:3, total concentration at 10 mg L^{-1}) over the as-prepared $\text{Bi}_4\text{O}_5\text{Br}_2$ and $\text{I}_x\text{-}\text{Bi}_4\text{O}_5\text{Br}_2$ samples were determined under visible-light irradiation (Fig. 8A and B). Their corresponding reaction rate constants were calculated according to Eq. (2) and are presented in Fig. 8C and D and Table 2. $\text{Bi}_4\text{O}_5\text{Br}_2$ showed a minor decline in degradation efficiency for the mixture of parabens, while $\text{I}_{0.7}\text{-}\text{Bi}_4\text{O}_5\text{Br}_2$ and $\text{I}_{1.0}\text{-}\text{Bi}_4\text{O}_5\text{Br}_2$ showed almost the same photodegradation efficiencies of MeP and PrP in the mixed solution as single MeP and PrP, which means that I-doped $\text{Bi}_4\text{O}_5\text{Br}_2$ can effectively degrade a mixture of parabens and that there is little influence between the parabens during this process.

Both reusability and stability of a catalyst are important for high-performance photocatalysts. As shown in Fig. 9A, $\text{I}_{0.7}\text{-}\text{Bi}_4\text{O}_5\text{Br}_2$ sample maintained high performances within seven reaction cycles (once a day for a week). In addition, the XRD analysis verified that its structure remained unchanged after the photocatalytic reaction (Fig. 9B). Thus, the $\text{I}_{0.7}\text{-}\text{Bi}_4\text{O}_5\text{Br}_2$ photocatalyst prepared using this facile and fast microwave method is excellent for the photocatalytic degradation of parabens under visible-light irradiation, which is important for its practical applications.

3.3. Photocatalytic degradation mechanisms

To understand the mechanism of the photocatalytic decomposition of the parabens over I-doped $\text{Bi}_4\text{O}_5\text{Br}_2$, theoretical calculations of the parabens were performed through molecular orbital theory [48] to determine their frontier-orbital energies. As shown in Table 3, with an increase in the length of the alkyl group (from MeP to BuP), the energy of the highest occupied molecular orbital (HOMO) decreased, the energy of the lowest unoccupied molecular orbital (LUMO) increased, and the energy difference between the LUMO and HOMO remained almost constantly at a high value of 5.40 eV. The oxidation potentials of the parabens can be predicted by the following equation (Eq. (3)) [32]:

$$E(\text{eV}) = -4.5 - E(\text{V}) \times 1 \text{ e} \quad (3)$$

where $E(\text{V})$ is the oxidation potential versus the normal hydrogen electrode (NHE), and $E(\text{eV})$ is the HOMO energy. Subsequently, the

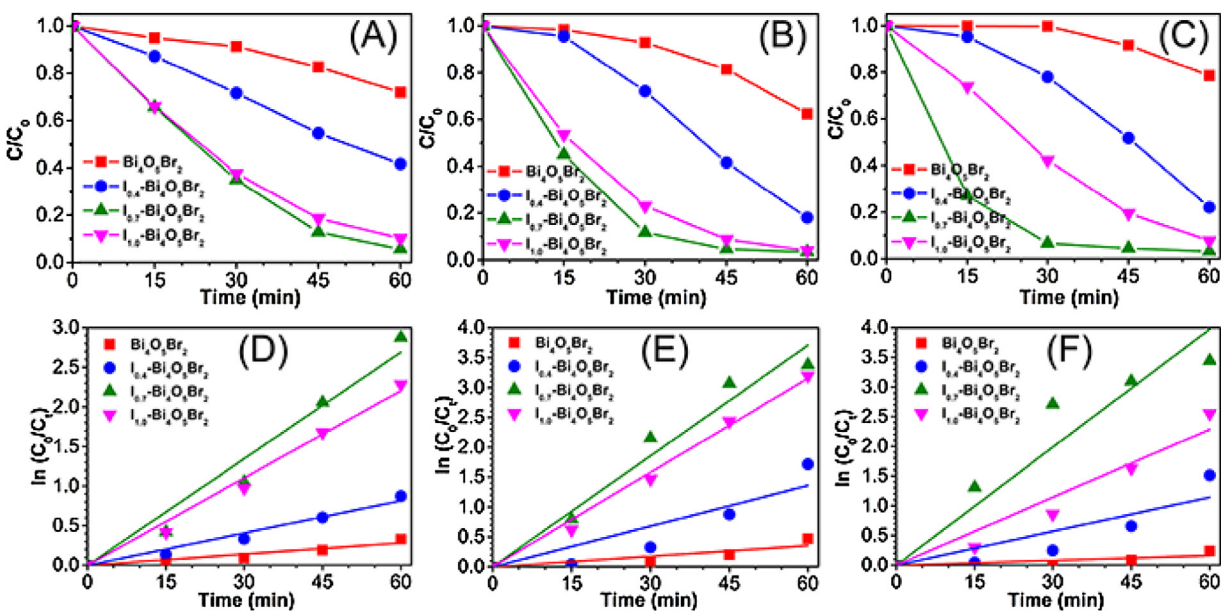


Fig. 7. Photocatalytic degradation of methylparaben (A), ethylparaben (B), and butylparaben (C) over $\text{I}_x\text{-Bi}_4\text{O}_5\text{Br}_2$ ($x = 0, 0.4, 0.7$ and 1.0) under visible-light irradiation; the corresponding linear plots of $\ln(C_0/C_t)$ versus degradation time (D-F).

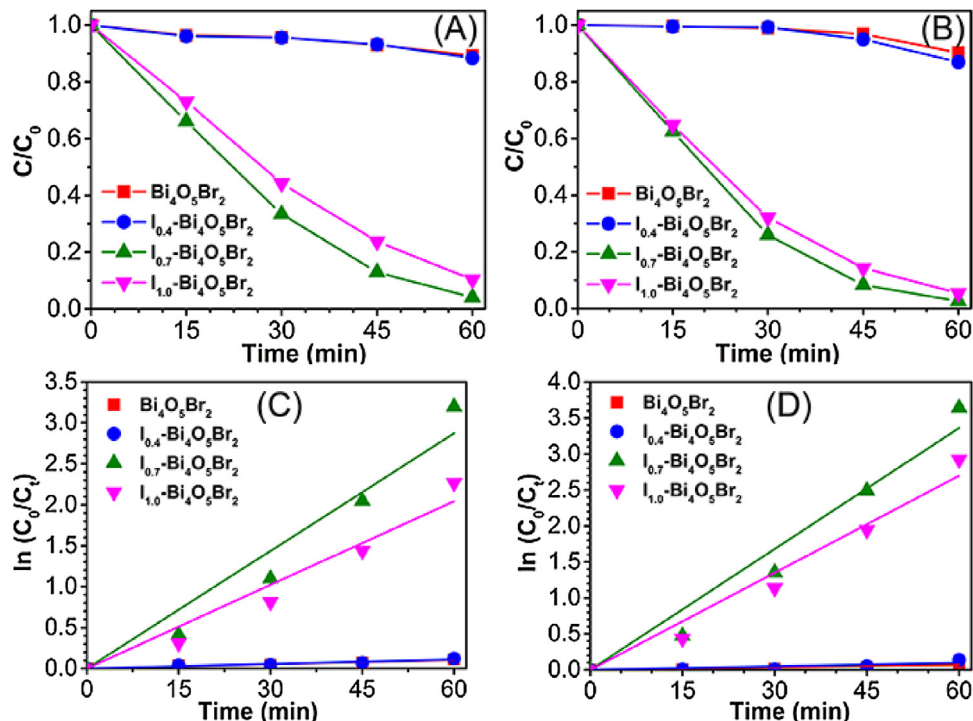


Fig. 8. Photocatalytic degradation of methylparaben (A) and propylparaben (B) in a mixture with a ratio of 1:3 over $\text{Bi}_4\text{O}_5\text{Br}_2$ and $\text{I}_x\text{-Bi}_4\text{O}_5\text{Br}_2$ ($x = 0.4, 0.7$, and 1.0) under visible-light irradiation; the corresponding linear plots of $\ln(C_0/C_t)$ versus degradation time (C and D).

oxidation potentials of MeP, EtP, PrP, and BuP were calculated to be 1.819, 1.794, 1.788, and 1.779 V, respectively, revealing that these compounds are rather stable and that their oxidation potentials are relatively high and decrease with an increasing length of alkyl substituents from methyl to butyl.

On the other hand, the valence-band energy of the as-synthesized photocatalysts can be evaluated according to the empirical equation (Eq. (4)) [49]:

$$E_{VB} = X - E^e + 0.5 E_g \quad (4)$$

where X is the absolute electronegativity of the semiconductor, E^e is the energy of the free electrons on the hydrogen scale, E_g is the band-gap energy of the semiconductor acquired from the DRS analysis, and E_{VB} is the valence-band potential of the photocatalyst. At different pH values, the E_{VB} can be further calculated according to the equation (Eq. (5)) [50]:

$$E = E^0 - 0.05915 \times \text{pH} \quad (5)$$

Accordingly, E_{VB} of as-prepared $\text{Bi}_4\text{O}_5\text{Br}_2$ is 2.45 V vs. NHE at pH = 7. Similarly, $\text{I}_{0.4}\text{-Bi}_4\text{O}_5\text{Br}_2$, $\text{I}_{0.7}\text{-Bi}_4\text{O}_5\text{Br}_2$, and $\text{I}_{1.0}\text{-Bi}_4\text{O}_5\text{Br}_2$,

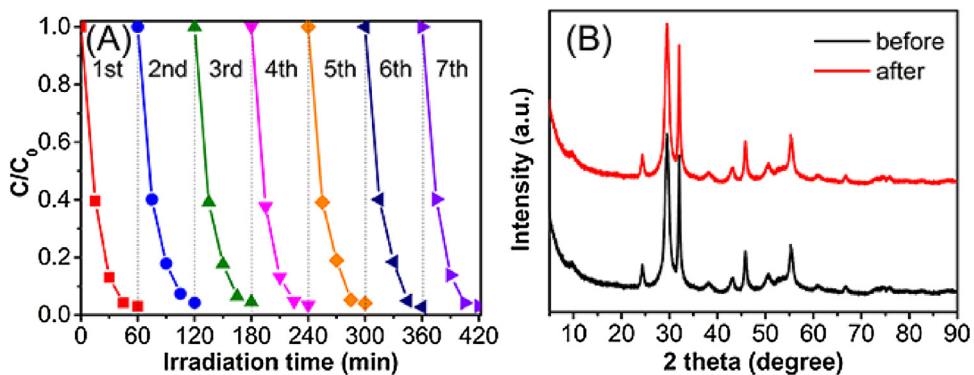


Fig. 9. (A) Recycling stability of the photocatalytic degradation of propylparaben over as-synthesized $I_{0.7}$ -doped $Bi_4O_5Br_2$; (B) XRD patterns of the as-synthesized $I_{0.7}$ -doped $Bi_4O_5Br_2$ sample before and after the photocatalytic reaction.

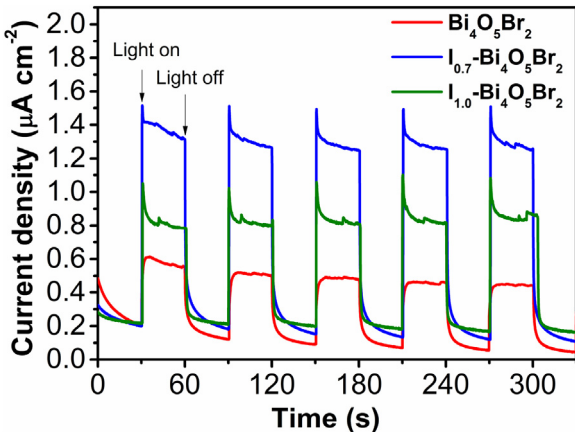


Fig. 10. Transient-photocurrent responses for as-synthesized $Bi_4O_5Br_2$, $I_{0.7}$ - $Bi_4O_5Br_2$, and $I_{1.0}$ - $Bi_4O_5Br_2$.

which have actual compositions of $Bi_4O_5Br_{1.8}I_{0.2}$, $Bi_4O_5Br_{1.4}I_{0.6}$, and $Bi_4O_5Br_{1.2}I_{0.8}$ according to the XPS quantitative analysis, have E_{VB} of 2.39, 2.36, and 2.15 V, respectively. With an increase in I doping amount, the valence-band potential of the photocatalyst decreases gradually. The valence-band potential difference between them are very close to those of the VB XPS (Fig. 5D). Importantly, the valence-band potentials of all these photocatalysts are higher than the oxidative potentials of the parabens, implying that it is thermodynamically possible for them to oxidize the parabens.

To explain the enhanced photocatalytic performances over I-doped $Bi_4O_5Br_2$, especially $I_{0.7}$ - $Bi_4O_5Br_2$, photocurrent experiments were performed. As shown in Fig. 10, $I_{0.7}$ - $Bi_4O_5Br_2$ displayed the strongest transient-photocurrent response, whereas the photocurrent response of pure $Bi_4O_5Br_2$ was rather poor, indicating that $I_{0.7}$ - $Bi_4O_5Br_2$ has the highest separation efficiency of photogenerated electron-hole pairs. Taken into account of the DRS and BET results, the I-doped $Bi_4O_5Br_2$ samples achieved superior photocatalytic activities to pure $Bi_4O_5Br_2$, which may arise from their more efficient separation of photogenerated electron-hole pairs, larger specific surface area, and better absorption in the visible-light region. The slightly reduced activity of $I_{1.0}$ - $Bi_4O_5Br_2$ is attributed to its lower valence-band potential and relatively poor separation of photoinduced carriers since the excess dopants can act as recombination centers.

As it is well known, the photogenerated reactive species, including electrons (e^-), holes (h^+), hydroxyl radicals ($\cdot OH$), and superoxide radicals ($\cdot O_2^-$), play important roles in photocatalytic reactions. To gain insights into the contributions of various reac-

tive species to the photodegradation of the parabens over the as-synthesized $I_{0.7}$ - $Bi_4O_5Br_2$ catalyst under visible-light irradiation, radical-scavenger experiments were performed by adding various scavengers into the system. As illustrated in Fig. 11A, after the addition of isopropanol as a scavenger for $\cdot OH$, the photodegradation efficiency of PrP remained almost the same, demonstrating the minor role of $\cdot OH$ in this process. This result may be ascribed to the standard redox potential of Bi^{5+}/Bi^{3+} ($E^0 = 1.59$ V at pH 0) that is more negative than that of $\cdot OH/OH^-$ ($E^0 = 1.99$ V at pH 0) and $\cdot OH/H_2O$ (2.73 eV at pH 0). Thus, the photogenerated holes cannot oxidize ambient OH^- or H_2O to yield $\cdot OH$ [51]. The photodegradation activity declined somewhat after silver nitrate was added to capture photogenerated electrons (e^-), implying that e^- may participate in the photodegradation process. However, a significant reduction in the photocatalytic performance was observed in the presence of sodium oxalate, and an obvious inhibition of the photocatalytic performance was also found when TEMPOL was added to quench $\cdot O_2^-$. These observations indicate that the photoreaction process in this system is dominated by h^+ and $\cdot O_2^-$. The redox potential of $O_2/\cdot O_2^-$ is -0.33 V vs. NHE, and the photogenerated electrons in the bottom of the CB of the as-prepared $I_{0.7}$ - $Bi_4O_5Br_2$ (-0.15 V calculated by $E_{VB}-E_g$) cannot yield $\cdot O_2^-$. However, under visible-light irradiation ($\lambda \geq 420$ nm and $E \leq 2.95$ eV), some electrons in the valence band of $I_{0.7}$ - $Bi_4O_5Br_2$ can be excited to high-energy states in the conduction band (up to -0.56 V). Consequently, $\cdot O_2^-$ could be formed by the reaction of these higher-energy electrons with dissolved oxygen. Therefore, the process of the photoreaction is mainly dominated by oxidation from photogenerated holes and superoxide radicals rather than $\cdot OH$.

The existence of $\cdot O_2^-$ can be further confirmed through EPR (Fig. 11B). The characteristic EPR signal of DMPO- $\cdot O_2^-$ can be clearly identified over $I_{0.7}$ - $Bi_4O_5Br_2$ under visible-light irradiation, and the intensity enhanced with the irradiation time. On the other hand, the characteristic peak of DMPO- $\cdot OH$ cannot be obviously detected under the identical conditions, and only a weaken signal was observed after 16 min of irradiation, which is consistent with the scavenger experiments. The trace $\cdot OH$ is derived from $\cdot O_2^-$ reacting with H^+ .

The TOC was selected as a mineralization index for the complete degradation of PrP over the $I_{0.7}$ -doped $Bi_4O_5Br_2$ during the photocatalytic process. Fig. S2 (Supporting Information) shows that more than 64% TOC was eliminated after visible-light photodegradation in 60 min. If the reaction time was prolonged to 180 min, approximately 80% TOC was removed, which is better than previously reported [14,31]. In addition, a small quantity of CO could be detected, and its amount increases with the reaction time, indi-

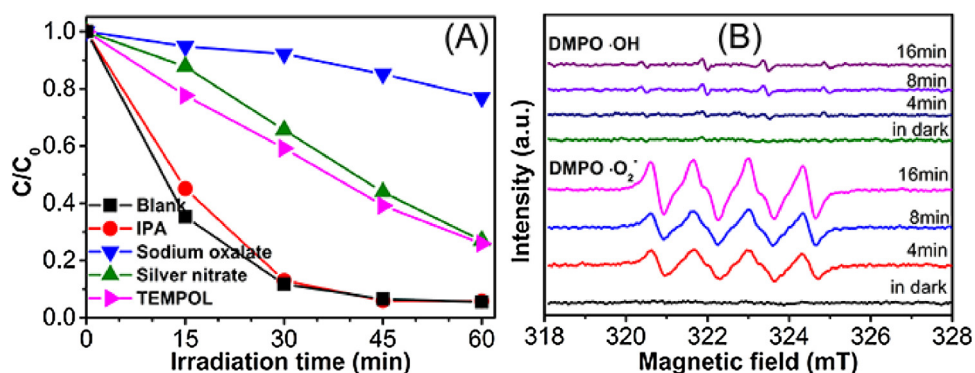


Fig. 11. (A) Photodegradation of propylparaben over as-synthesized $I_{0.7}$ -doped $Bi_4O_5Br_2$ in the presence of various scavengers: no scavenger (blank), isopropanol (IPA), sodium oxalate, silver nitrate, and 4-hydroxy-2,2,6,6-tetramethylpiperidinyloxy (TEMPOL); (B) DMPO spin-trapping EPR spectra for DMPO-•OH and DMPO-•O₂⁻ under visible-light irradiation over the $I_{0.7}$ -doped $Bi_4O_5Br_2$ photocatalyst.

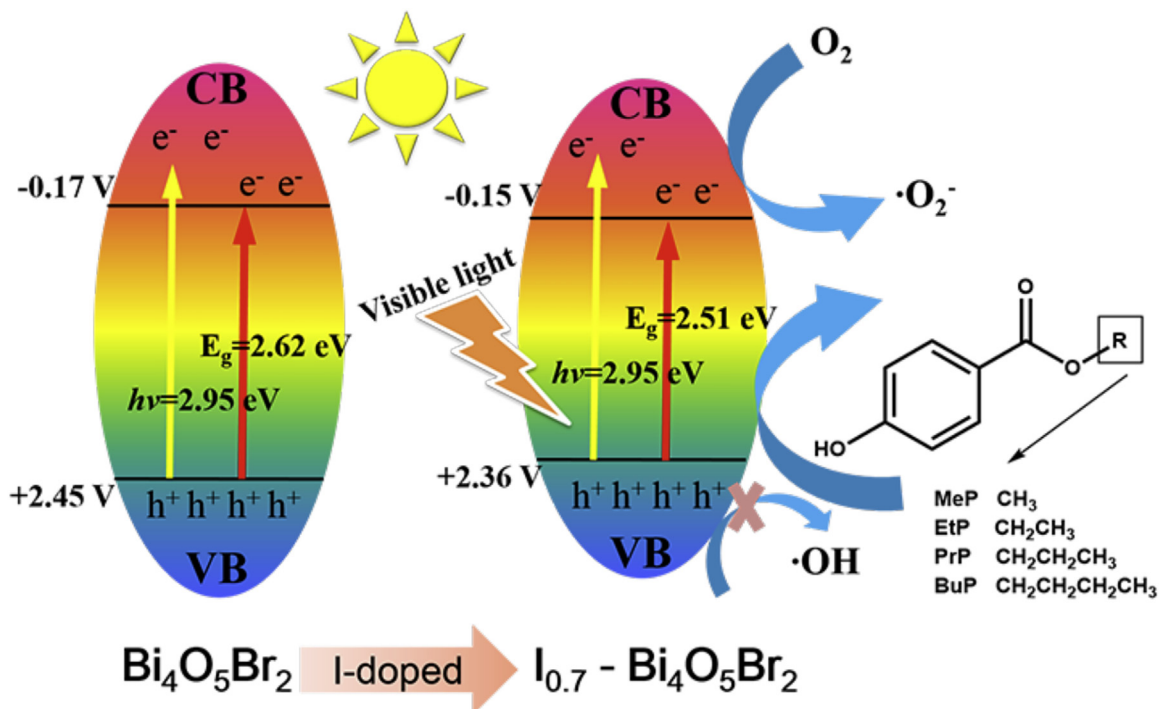
cating that the photocatalytic mineralization of organic pollutants over the $I_{0.7}$ -doped $Bi_4O_5Br_2$ catalyst underwent via CO.

Based on the above analyses, a photocatalytic reaction mechanism for the photodegradation of parabens over $I_{0.7}$ - $Bi_4O_5Br_2$ under visible-light irradiation is proposed in **Scheme 1**. Under visible-light irradiation ($\lambda \geq 420$ nm, at which the energy of light reaches the maximum of 2.95 eV), the light excites $I_{0.7}$ - $Bi_4O_5Br_2$ (band gap = 2.51 eV) to produce photogenerated carriers. The electrons in the valence band (2.36 V vs. NHE) of $I_{0.7}$ - $Bi_4O_5Br_2$ can be excited to high-energy states in the conduction band (up to -0.56 V vs. NHE) and afterwards react with dissolved oxygen to form $\bullet O_2^-$ for photocatalytic degradation process. The potential of the photogenerated holes of $I_{0.7}$ - $Bi_4O_5Br_2$ is higher than the oxidation potential of the parabens (approximately 1.8 V vs. NHE), and therefore, the parabens will lose electrons to form carbon radicals and then be further oxidized by the superoxide radicals. Compared with $Bi_4O_5Br_2$, $I_{0.7}$ - $Bi_4O_5Br_2$ can yield more oxidized species (i.e., photogenerated holes and superoxide radicals) under visible-light irradiation and

possesses a larger specific surface area, and thus has a significantly enhanced activity for the photocatalytic removal of parabens.

4. Conclusion

Excellent visible-light photocatalytic degradations of four parabens (MeP, EtP, PrP, and BuP) and mixture of parabens were found for the first time using novel I-doped $Bi_4O_5Br_2$ photocatalysts fabricated by a convenient and rapid microwave route. The significantly enhanced photocatalytic performances of the as-prepared $I_{0.7}$ - $Bi_4O_5Br_2$ sample were ascribed to the more efficient separation of photogenerated carriers, larger specific surface area, good visible-light absorption ($\lambda \leq 510$ nm), and positive valence-band edge potential (2.36 V vs. NHE). Photogenerated holes and superoxide radicals were confirmed to be the key reactive species in the photocatalytic process. Furthermore, the as-synthesized $I_{0.7}$ - $Bi_4O_5Br_2$ showed a good stability and potential for practical applications in environmental purification.



Scheme 1. Schematic illustration of the photocatalytic reaction mechanism for the photodegradation of parabens over $I_{0.7}$ -doped $Bi_4O_5Br_2$ under visible-light irradiation.

Acknowledgments

This work was financially supported by the National Natural Science Foundation of China (No. 21477040) and the Guangdong Province Natural Science Foundation (No. 2015A030313393, S2012040007074).

Appendix A. Supplementary data

Supplementary data associated with this article can be found, in the online version, at <http://dx.doi.org/10.1016/j.apcatb.2017.06.074>.

References

- [1] P.D. Darbre, Best Pract. Res. Clin. Endocrinol. Metab. 20 (2006) 121–143.
- [2] X. Feng, Y. Chen, Y. Fang, X. Wang, Z. Wang, T. Tao, Y. Zuo, Sci. Total Environ. 472 (2014) 130–136.
- [3] D. Błędzka, J. Gromadzińska, W. Wąsowicz, Environ. Int. 67 (2014) 27–42.
- [4] X. Peng, Y. Yu, C. Tang, J. Tan, Q. Huang, Z. Wang, Sci. Total Environ. 397 (2008) 158–166.
- [5] R.A. Rudel, D.E. Camann, J.D. Spengler, L.R. Korn, J.G. Brody, Environ. Sci. Technol. 37 (2003) 4543–4553.
- [6] L. Núñez, J.L. Tadeo, A.I. García-Valcárcel, E. Turiel, J. Chromatogr. A 1214 (2008) 178–182.
- [7] X. Ye, A.M. Bishop, L.L. Needham, A.M. Calafat, Anal. Chim. Acta 622 (2008) 150–156.
- [8] I. Jiménez-Díaz, F. Vela-Soria, A. Zafra-Gómez, A. Navalón, O. Ballesteros, N. Navea, M.F. Fernández, N. Olea, J.L. Vilchez, Talanta 84 (2011) 702–709.
- [9] G. Shanmugam, B.R. Ramaswamy, V. Radhakrishnan, H. Tao, J. Microchem. (2010) 391–396.
- [10] M.G. Soni, G.A. Burdock, S.L. Taylor, N.A. Greenberg, Food Chem. Toxicol. 39 (2001) 513–532.
- [11] S. Oishi, Toxicol. Ind. Health 17 (2001) 31–39.
- [12] P.D. Darbre, A. Aljarrah, W.R. Miller, N.G. Coldham, M.J. Sauer, G.S. Pope, J. Appl. Toxicol. 24 (2004) 5–13.
- [13] E.J. Routledge, J. Parker, J. Odum, J. Ashby, J.P. Sumpter, Toxicol. Appl. Pharm. 153 (1998) 12–19.
- [14] Y. Lin, C. Ferronato, N. Deng, F. Wu, J. Chovelon, Appl. Catal. B: Environ. 88 (2009) 32–41.
- [15] N. Jonkers, H.E. Kohler, A. Dammshäuser, W. Giger, Environ. Pollut. 157 (2009) 714–723.
- [16] A. Kubacka, M. Fernández-García, G. Colón, Chem. Rev. 112 (2012) 1555–1614.
- [17] S. Esplugas, D.M. Bila, L.G.T. Krause, M. Dezotti, J. Hazard. Mater. 149 (2007) 631–642.
- [18] Y. Lin, C. Ferronato, N. Deng, J. Chovelon, Appl. Catal. B: Environ. 104 (2011) 353–360.
- [19] H. Fang, Y. Gao, G. Li, J. An, P. Wong, H. Fu, S. Yao, X. Nie, T. An, Environ. Sci. Technol. 47 (2013) 2704–2712.
- [20] P. Atheba, P. Drogui, B. Seyhi, D. Robert, Water Sci. Technol. 67 (2013) 2141–2147.
- [21] A. Petala, Z. Frontistis, M. Antonopoulou, I. Konstantinou, D.I. Kondarides, D. Mantzavinos, Water Res. 81 (2015) 157–166.
- [22] X. Liu, H. Cao, J. Yin, Nano Res. 4 (2011) 470–482.
- [23] X. Xiao, R. Hu, C. Liu, C. Xing, C. Qian, X. Zuo, J. Nan, L. Wang, Appl. Catal. B: Environ. 140–141 (2013) 433–443.
- [24] S. Cao, P. Zhou, J. Yu, Chin. J. Catal. 35 (2014) 989–1007.
- [25] H. Lan, G. Zhang, H. Zhang, H. Liu, R. Liu, J. Qu, Catal. Commun. 98 (2017) 9–12.
- [26] X. Lou, J. Shang, L. Wang, H. Feng, W. Hao, T. Wang, Y. Du, J. Mater. Sci. Technol. 33 (2016) 281–284.
- [27] Y. Zhang, M. Park, H.Y. Kim, B. Ding, S. Park, Appl. Surf. Sci. 384 (2016) 192–199.
- [28] X. Wang, W. Bi, P. Zhai, X. Wang, H. Li, G. Mailhot, W. Dong, Appl. Surf. Sci. 360 (2016) 240–251.
- [29] S. Han, J. Li, K. Yang, J. Lin, Chin. J. Catal. 36 (2015) 2119–2126.
- [30] S. Tu, M. Lu, X. Xiao, C. Zheng, H. Zhong, X. Zuo, J. Nan, RSC Adv. 6 (2016) 44552–44560.
- [31] X. Xiao, R. Hu, S. Tu, C. Zheng, H. Zhong, X. Zuo, J. Nan, RSC Adv. 5 (2015) 38373–38381.
- [32] X. Xiao, S. Tu, M. Lu, H. Zhong, C. Zheng, X. Zuo, J. Nan, Appl. Catal. B: Environ. 198 (2016) 124–132.
- [33] Y. Bai, T. Chen, P. Wang, L. Wang, L. Ye, J. Chem. Eng. (2016) 454–460.
- [34] M. Li, Y. Cui, Y. Jin, H. Li, RSC Adv. 6 (2016) 47545–47551.
- [35] J. Di, J. Xia, M. Ji, S. Yin, H. Li, H. Xu, Q. Zhang, H. Li, J. Mater. Chem. A 3 (2015) 15108–15118.
- [36] Y. Bai, L. Ye, T. Chen, P. Wang, L. Wang, X. Shi, P.K. Wong, Appl. Catal. B: Environ. 203 (2017) 633–640.
- [37] Y. Yang, H. Wang, X. Li, C. Wang, Mater. Lett. 63 (2009) 331–333.
- [38] C. Zheng, G. He, X. Xiao, M. Lu, H. Zhong, X. Zuo, J. Nan, Appl. Catal. B: Environ. 205 (2017) 201–210.
- [39] X. Xiao, W. Zhang, RSC Adv. 1 (2011) 1099–1105.
- [40] X. Zhang, Z.H. Ai, F.L. Jia, L.Z. Zhang, J. Phys. Chem. C 112 (2008) 747–753.
- [41] F. Qin, G. Li, R. Wang, J. Wu, H. Sun, R. Chen, J. Chem. Eur. 18 (2012) 16491–16497.
- [42] L.Q. Ye, X.L. Jin, C. Liu, C.H. Ding, H.Q. Xie, K.H. Chu, P.K. Wong, Appl. Catal. B: Environ. 187 (2016) 281–290.
- [43] X. Xiao, C. Xing, G. He, X. Zuo, J. Nan, L. Wang, Appl. Catal. B: Environ. 148–149 (2014) 154–163.
- [44] S.J. Genuis, D. Birkholz, L. Curtis, ISRN toxicol. 2013 (2013) 507897.
- [45] J. Xu, W. Meng, Y. Zhang, L. Li, C. Guo, Appl. Catal. B: Environ. 107 (2011) 355–362.
- [46] E.M. Cuerda-Correa, J.R. Dominguez, M.J. Munoz-Pena, T. Gonzalez, Ind. Eng. Chem. Res. 55 (2016) 5161–5172.
- [47] E.M. Cuerda-Correa, J.R. Dominguez-Vargas, M.J. Munoz-Pena, T. Gonzalez, Ind. Eng. Chem. Res. 55 (2016) 5152–5160.
- [48] N. San, A. Hatipoğlu, G. Koçtürk, Z. Çınar, J. Photochem. Photobiol. A: Chem. 146 (2002) 189–197.
- [49] Y. Xu, M.A.A. Schoonen, Am. Mineral. 85 (2000) 543–556.
- [50] J. Cao, B. Xu, H. Lin, B. Luo, S. Chen, Dalton Trans. 41 (2012) 11482–11490.
- [51] Y. Li, J. Wang, H. Yao, L. Dang, Z. Li, J. Mol. Catal. A: Chem. 334 (2011) 116–122.